Mechanism of the exchange-bias field in ferromagnetic and antiferromagnetic bilayers

C. Mitsumata* and A. Sakuma
Advanced Electronics Research Laboratory, Hitachi Metals Ltd., 5200 Mikajiri, Kumagaya, Saitama 360-0843, Japan

K. Fukamichi
Department of Materials Science, Graduate School of Engineering, Tohoku University, Aoba-yama 02, Sendai 980-8579, Japan
(Received 28 November 2002; revised manuscript received 26 March 2003; published 31 July 2003)

Exchange-bias field phenomena in ferromagnetic and antiferromagnetic bilayers have been investigated by means of the Monte Carlo calculations within the framework of the classical Heisenberg model. The calculations for a binary alloy composed of magnetic and nonmagnetic atoms such as a disordered γ-phase antiferromagnetic layer show a noncollinear spin structure. In addition, the calculated magnetization process gives a loop shift due to the unidirectional exchange-bias field. In other words, the noncollinear spin structure caused by the geometric frustrations in the antiferromagnetic layer is responsible for the magnetization loop shift. On the other hand, a collinear spin structure formed in an ordered $L1_0$-type antiferromagnetic alloy results in only the enhancement of coercivity of the ferromagnetic layer. Introducing the multidomains into the ordered $L1_0$-type antiferromagnetic layer, however, the magnetization loop shift of the ferromagnetic layer is evidently developed by the geometrically frustrated spins induced at the magnetic domain boundaries.

DOI: 10.1103/PhysRevB.68.014437 PACS number(s): 75.10.Hk, 75.25.+z, 75.30.Et, 75.40.Mg

I. INTRODUCTION

Since the first observation by Meiklejohn and Bean[1] for the exchange-bias field phenomena at the interface between ferromagnetic (FM) and antiferromagnetic (AFM) materials, many theoretical models have been proposed. The approaches of discrete micromagnetics models,[2–8] continuum micromagnetics models,[9–12] and others[13–17] have tried to explain the exchange-bias field phenomenon qualitatively and quantitatively. The Ising spin and the square lattice were considered in the model of Malozemoff,[2] and the presence of the AFM domain causes the exchange-bias field. Another quantitative explanation was given by Mauri *et al.*[9] and the vector spin was considered to form the magnetic domain wall at the interface between the FM and the AFM layers. The influence of the competition between the FM and the AFM interactions was first shown by Koon[3] by using a b.c.c lattice with the vector spin. Such a competition is accompanied by the relaxation of spins and the ''spin-flop state'' at the interface.

The ''random-field model'' by Malozemoff[2] contrasts with the spin-flop model by Koon[3] for the explanation of the origin of an exchange-bias field at the ''compensated interface.'' The compensated interface is formed by the spin configuration, where the magnetization is canceled out due to the summation of the positive and negative components of spins in the AFM layer. The random-field model requires the atomic roughness of the interface, whereas in the spin-flop model the interface roughness is not required but a domain wall structure parallel to the interface is necessary, which was first introduced by Mauri *et al.*[9] Those models explain the appearance of a magnetization loop shift in a FM/AFM bilayer. Later on, Schulthess and Butler[4,5] pointed out that there is a possibility of different process in the spin flop. According to their calculation, the perpendicular component of the spin vector to the interface becomes finite during the magnetization reversal process (hereafter, we call ''3D reversal,'' where 3D is three dimensional) in the FM layer, and this spin-flip model can cause no magnetization loop shift. Also, they pointed out that the solution by Koon is held in the restriction of the in-plane magnetization reversal (hereafter, we call ''2D reversal'') accompanied by the unidirectional exchange-bias field. The calculation by Xi and White[11] is in conflict with the 2D reversal. However, it should be noted that all those discussions are based on the collinear spin structure in AFM layers. For practical applications, the alloy systems used as an AFM layer usually exhibit a variety of the spin structures, including the collinear and noncollinear antiferromagnetic spin arrangements. For example, ordered $L1_0$-type MnNi and MnPt alloys have an AF-I-type collinear spin structure,[18–20] while disordered γ-phase Mn-Ni, Mn-Rh, and Mn-Ir alloys have the noncollinear type of a triple-Q ($\equiv 3Q$) spin structure.[21,22] In both cases, the unidirectional exchange bias field is observed experimentally.[23–32] Note that various theoretical and experimental works have been reviewed by Berkowitz and Takano.[33]

For both the collinear and noncollinear antiferromagnetic spin structures, the question arises whether the unidirectional exchange-bias field is caused by the same mechanism or not. In the present study, we intend to elucidate the mechanism of the magnetization loop shift in the FM/AFM bilayer, focusing on the influence of the realistic spin structure in the AFM layer. Then, we demonstrate that the same motive force causes the unidirectional exchange-bias field in not only the collinear but also in noncollinear spin systems. From these results, it should be emphasized that the frustrated spins due to the geometric arrangement of the AFM atoms are essential to develop the exchange-bias field.

II. MODEL OF CALCULATIONS

The configuration of atoms in the present model is illustrated in Fig. 1. The bilayer is constructed of the $\langle 111 \rangle$ stacking in the triangular net plane, forming a compensated interface between the FM and the AFM layers. The closed and

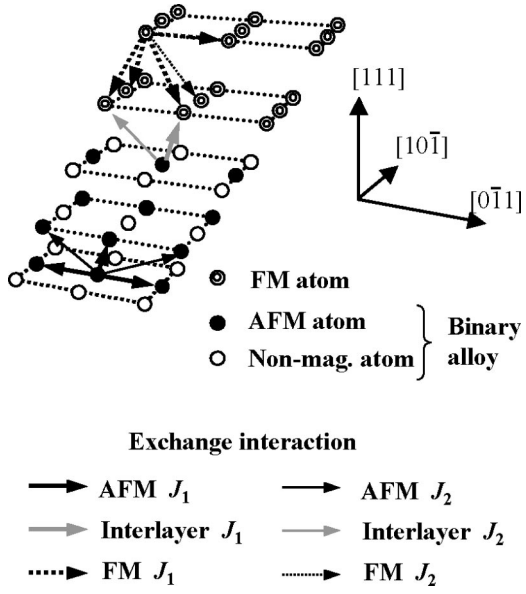

FIG. 1. The model lattice of the FM and AFM bilayer.

open circles represent the magnetic and nonmagnetic atoms in the AFM layer, respectively, composing a binary alloy. The atomic configuration in Fig. 1 corresponds to the case of an ordered $L1_0$-type AFM layer. For the disordered γ-phase AFM layer, the lattice becomes an f.c.c. structure. The double circles denote the magnetic atoms in the FM layer. The layer thickness of the FM layer is 9 ML (monolayer), corresponding to about 15 Å for typical FM layers, e.g., Ni, Fe, and Co. On the other hand, the AFM layer thickness ranges from 10 to 120 ML. The interface between the FM and the AFM layers is clearly defined without any roughness. The periodic boundary condition is applied to the in-plane direction of the layered film and the calculated region includes 24×24 atoms in each monolayer (ML).

To investigate the spin structures and the magnetization process of the FM/AFM bilayer, the classical Heisenberg model is adopted in the present paper. Within the framework of this model, we consider the interactions up to the second nearest neighbors because the interaction between the second nearest neighbors plays an important role to establish long-range order; the antiferromagnetic spin arrangement in frustrated spin systems in the present case. The thick arrows stand for the exchange interaction J_1 between the first nearest-neighboring spins and the dashed arrows represent the FM exchange interaction. The thin arrows indicate the exchange interaction J_2 between the second nearest-neighboring spins and the dashed arrows represent the FM exchange interaction as well. In the present classical Heisenberg model, we assume that the interlayer exchange constant is equal to the exchange constant in the AFM layer. The total magnetic energy is given by the following Hamiltonian.

$$H=-\sum_{\langle i,j\rangle} J_{1_{ij}}\boldsymbol{S}_i\cdot\boldsymbol{S}_j-\sum_{\langle i,k\rangle} J_{2_{ik}}\boldsymbol{S}_i\cdot\boldsymbol{S}_k-\sum_i D_i(\boldsymbol{S}_i\cdot\boldsymbol{n})^2$$

$$-g\mu_{\mathrm{B}}\sum_i(\boldsymbol{H}_{\mathrm{d}_i}+\boldsymbol{H}_{\mathrm{app}})\cdot\boldsymbol{S}_i, \qquad (1)$$

where S_i is the unit spin vector of the ith magnetic atom, J_1 and J_2 are the exchange constants for the first and the second nearest neighbors, respectively. The summations $\langle i,j\rangle$ and $\langle i,k\rangle$ are carried out over all possible pairs of the first and the second nearest neighbors. The third term in Eq. (1) represents the magnetic anisotropy energy, D_i and n mean the single spin anisotropy energy and the unit vector along the easy direction of the magnetic anisotropy, respectively. The last term in Eq. (1) describes the Zeeman energy, H_d is the demagnetized field due to the dipole interaction between spins, and H_{app} is the applied field. Typically, the exchange constants of magnetic alloys composed of Mn, Ni, Fe, and Co are of 10~30 meV, which can be estimated by the Néel temperature or the Curie temperature. For simplicity, in the present study, the first nearest exchange constant J_1 is assumed to be 20 meV for the FM layer and to be -20 meV for the AFM layer and the interface, and the second nearest exchange constant J_2 is given by $J_2=|J_1|/2$.[14] For the calculation of the demagnetized field H_d, the magnetic moment of the atom is assumed to be 1.7 μ_B like that of Co. For example, Ni-Fe or Co-Fe alloy is used for the FM layer in the FM/AFM bilayer system, and a typical anisotropy field of such alloys shows the order of 1~10 Oe. Accordingly, the anisotropy energy of 0.116 μeV corresponds to 10 Oe. The anisotropy energy of the AFM layer becomes $10^3\sim10^4$ times larger than that of the FM layer,[34] and hence, we assume 0.116 meV in the present study.

The single-spin-flip Metropolis algorithm is employed for the Monte Carlo calculations of the spin structures in the AFM layer system. First, 5×10^3 Monte Carlo steps are spent for the relaxation of the system and next 2×10^5 Monte Carlo steps are adopted as the Monte Carlo average for the physical observable. In addition, the Landau-Lifshitz motion equation is used to solve the magnetization process in the external applied field to the FM/AFM bilayer. The following Eq. (2) describes the motion equation:

$$\frac{d\boldsymbol{S}_i}{dt}=-\nu\boldsymbol{S}_i\times\boldsymbol{H}_{\mathrm{eff}_i}-\alpha[\boldsymbol{S}_i\times(\boldsymbol{S}_i\times\boldsymbol{H}_{\mathrm{eff}_i})], \qquad (2)$$

where $\boldsymbol{S}_i$ is the unit vector of the ith spin in the system and α is the damping constant. In the present calculations, we assume $\alpha=0.1$. The effective field at the ith site $\boldsymbol{H}_{\mathrm{eff}_i}$ is given by the following derivative of the Hamiltonian in Eq. (1):

$$\boldsymbol{H}_{\mathrm{eff}_i}=-\partial H/\partial\boldsymbol{S}_i. \qquad (3)$$

This motion equation is solved by using a forward difference method. The time step Δt in the difference equation is defined by $\Delta t=0.02/(\nu H_{app})$, where ν and H_{app} are the gyromagnetic constant and the applied field, respectively.

III. UNIDIRECTIONAL EXCHANGE-BIAS FIELD

The spin structure of the disordered AFM layer including 75% of magnetic atoms and 25% of nonmagnetic atoms in analogy with the disordered γ-phase Mn alloys is calculated by employing the Monte Carlo method in Fig. 2(a). Also, the spin structure of the disordered alloy with 97.5% of magnetic atoms and 2.5% of nonmagnetic atoms is calculated in Fig.

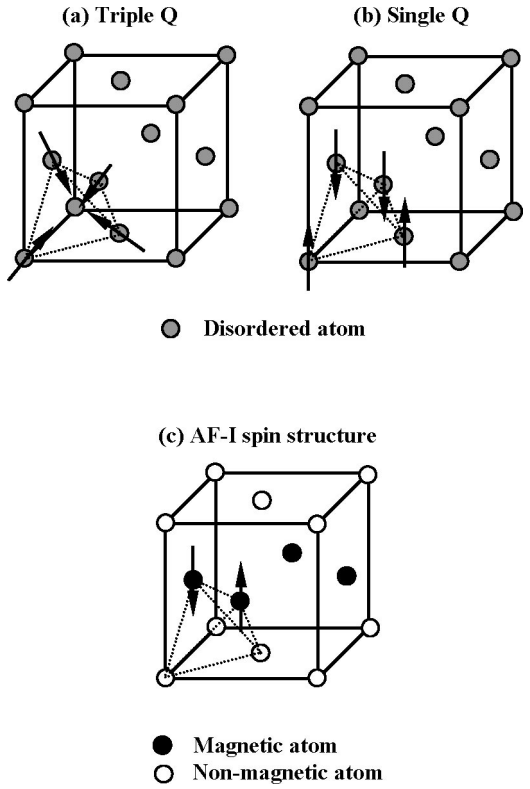

FIG. 2. The schematic drawing of the collinear and noncollinear spin structure in AFM alloys. (a) Triple-Q spin structure in the disordered γ-phase lattice, (b) single-Q spin structure in the disordered γ-phase lattice, (c) AF-I spin structure in the ordered $L1_0$-type lattice. The dashed lines represent the magnetic unit cell.

2(b). The atomic arrangements and the spin configurations in the AFM layers are illustrated in Fig. 2. The temperature used in the calculations is $T/J_1=0.086\,17$, giving the condition of $T \ll T_N$, the Néel temperature. In fact, the value of T_N/J_1 is 1.896 ± 0.038, 2.887 ± 0.053, and 3.567 ± 0.061 for Figs. 2(a), 2(b), and 2(c), respectively. The reason why we use such a value of T/J_1 is for the confirmation of the spin structures in the present model. Later on, as given in Fig. 3

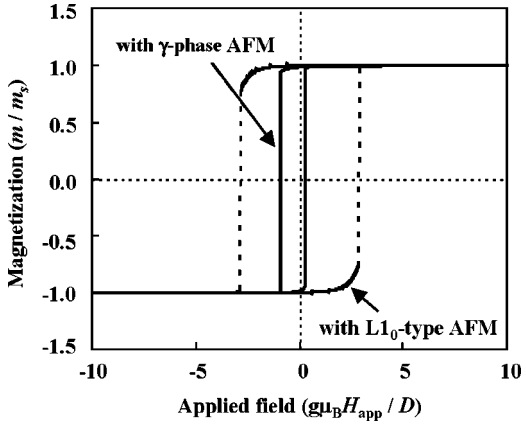

FIG. 3. The magnetization loops of the FM/AFM bilayer with the ordered $L1_0$-type (dashed lines) and the disordered γ-phase AFM alloys (bold lines).

and the succeeding discussion, we evaluate the exchange bias to use the motion equation of Landau-Lifshitz which is generally solved at 0 K. The shaded circles represent the disordered atoms. The closed and open circles denote the magnetic and nonmagnetic atoms, respectively. The arrows indicate the spin vectors and the dashed lines represent the magnetic unit cells. The spin vector is obtained by averaging the spins on the equivalent site:

$$\bar{\boldsymbol{S}}_I=\frac{1}{N}\sum_i \boldsymbol{S}_i, \quad \cos\theta=\langle \bar{\boldsymbol{S}}_I\cdot\bar{\boldsymbol{S}}_K\rangle, \tag{4}$$

where N is the number of magnetic atoms on each sublattice I. The correlation angle θ of the spin structures is calculated by a linear combination of averaged spins. The Néel temperatures in Fig. 2 are obtained from the following equation:

$$\left(\frac{\partial}{\partial T}\ln\langle \bar{S}_I\rangle\right)^{-1}=\frac{T-T_N}{\beta}, \tag{5}$$

where $\langle \bar{S}_I\rangle$ is the average size of the classical spin. In Figs. 2(a) and 2(b), it averages over four spins on the equivalent site $I(I=1,2,3,4)$. In Fig. 2(c), it averages over two spins on the equivalent site I ($I=1,2$ where 1, 2 are consisted of magnetic atoms). β is the critical exponent in the expansion equation of $m\propto(T-T_N)^{\beta}$ near the critical temperature. In the magnetic unit cell of a disordered γ-phase AFM layer in Fig. 2(a), four equivalent atoms are included, and the spins of those atoms point the $[111]$,$[\bar{1}\bar{1}1]$,$[1\bar{1}\bar{1}]$, and $[\bar{1}1\bar{1}]$ directions, respectively. This spin configuration corresponds to the $3Q$ spin structure which is a typical noncollinear spin structure in the f.c.c. lattice, resulting from the frustrated spins due to the atomic geometry.

Within the framework of the classical Heisenberg model, in principle, the ground-state energy of the collinear spin structure or the single Q ($\equiv 1Q$) structure in Fig. 2(b), is not distinguishable from the noncollinear spin structure of the $3Q$ structure, in the f.c.c. lattice[35,36] where all equivalent atoms are purely magneticlike γ-Mn. However, the presence of nonmagnetic atoms changes the number of interacting spins at the nearest neighboring atomic sites, causing the spin frustration in the disordered γ-phase alloy system. This spin frustration lowers the energy of the $3Q$ spin structure, compared with that of the collinear spin structure.[37] We have also confirmed the validity of this behavior to use the motion equation of spins. The initial spin configuration is assumed to be in the $1Q$ structure, and hence, the final solution is obtained to be the $3Q$ spin structure in the case of the disordered alloy with 75% of magnetic atoms and 25% of nonmagnetic atoms. The magnetic energy lowers from -120 to -126 meV/spin, changing the spin structure from $1Q$ to $3Q$. In addition, the spin configuration of the ordered AFM layer having the $L1_0$-type lattice structure is calculated by using the Monte Carlo method. In the present case, two magnetic and two nonmagnetic atoms are included in the magnetic unit cell as seen from Fig. 2(c). The spin correlation angle between the nearest-neighboring spins is 180° and it corresponds to the AF-I spin structure, being a typical collinear

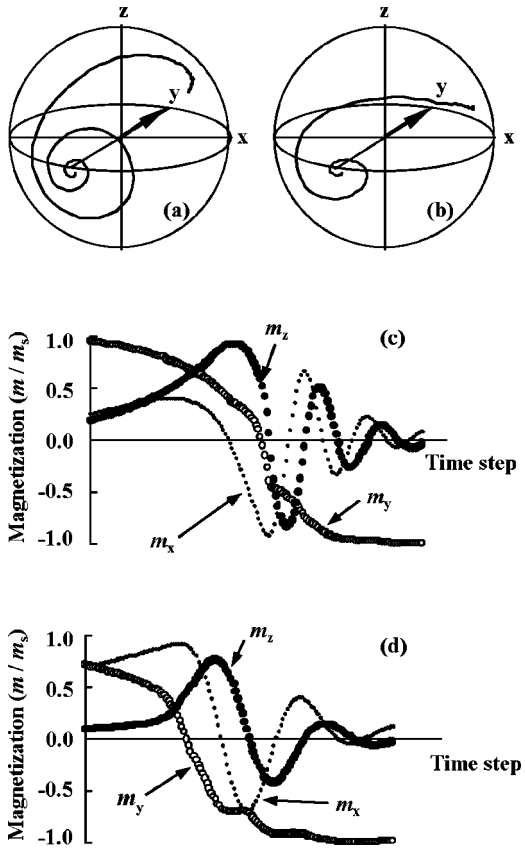

FIG. 4. The magnetization switching process in the FM layer of the FM/AFM bilayer with the ordered $L1_0$-type and the disordered γ-phase AFM alloys. (a) and (b) schematic images of the magnetization reversal with the ordered $L1_0$-type and the disordered γ-phase AFM alloys, respectively. (c) The magnetization in three components against the time step for the bilayer with the ordered $L1_0$-type AFM alloy having the collinear spin arrangement, (d) the same plots with the disordered γ-phase AFM alloy having the noncollinear spin arrangement.

spin structure of AFM alloys. Then, the magnetization process in an external field is calculated by adding the FM layer to such AFM layers.

The magnetization loop with the disordered γ-phase AFM layer is shifted by the unidirectional exchange-bias field, while the loop with the $L1_0$-type ordered AFM layer exhibits only the enhancement of coercivity instead of the bias field shift as shown in Fig. 3 where m_s is the saturation magnetization. In these cases, the magnetic easy directions in the AFM and FM layer are $[11\bar{2}]$ and $[\bar{1}10]$, respectively. These distinct different magnetization loops are explained in the following way. Each component of the magnetization vector m in the FM layer during the magnetization reversal process is plotted in Figs. 4(a) and 4(b) with the disordered γ-phase AFM and the ordered $L1_0$-type AFM layers, respectively. The x and y components lie down in the layered film, and the z-component is perpendicular to the film plane. The initial magnetization points the $+y$ direction and the switching field is applied to the $-y$ direction. While the y component m_y decreases from 1 to -1, m_x, and m_z oscillate and converge to zero, exhibiting the Larmor precession in the

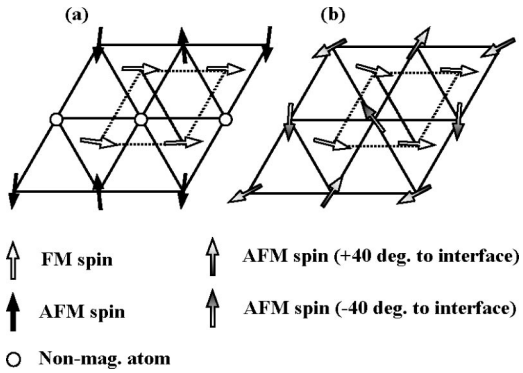

FIG. 5. The spin structures at the interface of bilayer system. (a) Ordered $L1_0$-type AFM layer and (b) disordered γ-phase AFM layer.

magnetization process. Let us focus on the m_z component for an ordered AFM layer having the AF-I spin structure in Fig. 4(a) and the case of a disordered γ-phase AFM layer having the $3Q$ spin structure in Fig. 4(b). In Figs. 4(c) and 4(d), the vertical axis denotes the magnetization in the x, y, and z components and the horizontal axis denotes the time step in the calculations. The m_z component in the former increases and makes the first peak of the oscillation before m_y crossing the zero line in Fig. 4(c), while m_z in the latter is restricted to a small value and makes the first peak after m_y crossing the zero lines in Fig. 4(d). The former corresponds to the 3D reversal and the latter does to the 2D reversal in the first half of the magnetization process. As a result, the magnetization loop shift is developed only in the bilayer system having the noncollinear spin structure.

As pointed out above, those switching modes are influenced by the spin structure of the AFM layer. Therefore, we investigate the spin structure at the interface. The correlation angle between the FM and the AFM spins indicates about 90° for the ordered AFM layer, and all of the FM and AFM spins lie down in the film plane. In Fig. 5(a), this spin structure is called the spin flop structure, and the spin correlation angle is likely to keep 90° during the whole magnetization reversal process. The FM spins show a 3D reversal with the perpendicular component to the interface because the AFM spins remain in the film plane. This is because the correlation angle between the FM and AFM spins corresponds to the bisection of the correlation angle between the AFM spins in a collinear configuration, and the switching path along such bisection gives the minimum state in the exchange energy. Next, we show the spin configuration at the interface with a disordered γ-phase AFM layer in Fig. 5(b). The FM spins lie in the film plane, but the perpendicular spin component to the interface presents in the γ-phase disordered AFM layer where the AFM spin meets $+40°$ or $-40°$ with the interface. The correlation angle between the FM and the AFM spins agrees with the bisection of the correlation angle between AFM spins, and it is also equivalent to the meeting angle of AFM spins to the interface. As a consequence, the direction of the FM spins is restricted near the parallel plane to the interface during the switching process. In other words, the FM spins with the disordered γ-phase AFM layer exhibit a 2D reversal.

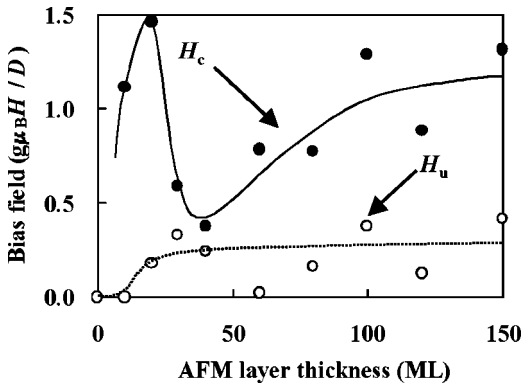

FIG. 6. The thickness dependence of the unidirectional exchange-bias field and coercivity with the disordered γ-phase FM/AFM bilayer. The unidirectional exchange-bias field and coercivity are given by H_{u} and H_{C}, respectively.

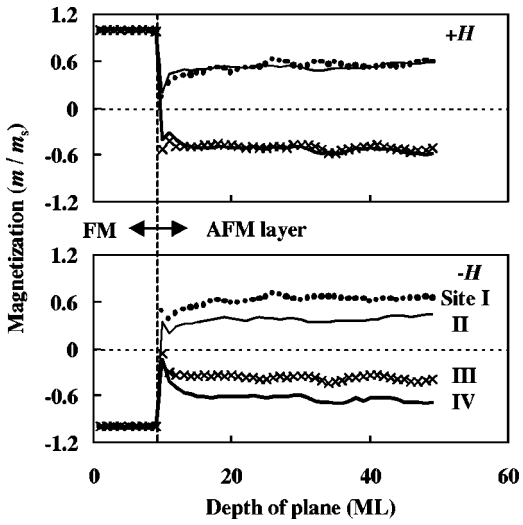

FIG. 7. The depth profile of magnetizations on the stacked planes with the disordered γ-phase FM/AFM bilayer. Four types of lines; dots, thin, cross, and thick, indicate the averaged magnetization of the equivalent atomic site, I, II, III, and IV in each stacked plane. The depth from 1 to 9 corresponds to the FM layer and that from 10 to 49 corresponds to the AFM layer.

IV. MAGNETIC DOMAIN WALL STRUCTURE IN THE AFM LAYER

The thickness dependence of the exchange-bias field in the bilayer system is shown in Fig. 6. Below about 25 ML, the unidirectional bias field H_u decreases when the AFM layer thickness ML decreases and it becomes zero below a certain critical thickness. The coercive force H_C takes a maximum value around such a critical thickness. The systematic error in the calculations of H_u and H_c is 0.005 in an normalized unit in Fig. 6, and the statistical error is about $+/-0.15$. These behaviors are very similar to the measured results for an FeMn film as the AFM layer,[16] which has been reported to have the $3Q$ spin structure.[38,39] The unidirectional exchange-bias field is influenced not only by the spin structure at the interface but also by the macroscopic spin arrangement in the AFM layer. The magnetization components m/m_s for four equivalent atoms along the applied field are plotted as a depth profile of the stacking films in Fig. 7. The magnetization of an equivalent atom is averaged over the net plane in each depth. The stacked planes in depth from 1 to 9 ML correspond to the FM layer and the stacked planes in depth from 10 to 49 ML correspond to the AFM layer. The magnetization in the FM layer stands $+1$ and -1 under the positive and negative applied fields, respectively. The value of m/m_s at each equivalent atom site, I, II, III, and IV, in the AFM layer is about $+0.5$ or -0.5, reflecting the correlation angle between the FM and the AFM spins. Approaching to the interface, the value of magnetization $|m|/m_s$ becomes small and forms the magnetic domain wall parallel to the interface, similar to the spin configuration presented by Mauri *et al.*,[9] and the domain wall shape is changed, depending on the direction of the applied field. Apparently, the change of the domain wall shape gives rise to the difference in the magnetic energy equivalent to the energy of the exchange-bias field.

V. INTRODUCTION OF MULTIDOMAINS INTO THE $L1_0$-TYPE AFM LAYER

In the preceding discussion, we have explained that the apparent magnetization loop shift is caused by the noncollinear spin structure, which is due to the random arrangement of magnetic and nonmagnetic atoms in the disordered γ-phase AFM alloys. In practical applications, however, the $L1_0$-type ordered AFM alloys such as MnPt,[23,24] MnNi,[25,26] and MnPdPt[40] perform excellent properties for the unidirectional exchange-bias field even though they have the collinear antiferromagnetic structure. Accordingly, at first glance, the present model seems to be invalid for the formation of unidirectional exchange-bias field in the collinear systems. We shall attempt to induce the spin frustration effect into the ordered $L1_0$-type AFM layer. For this purpose, we introduce the multidomains as illustrated in Fig. 8. Two magnetic atoms and two nonmagnetic atoms are included in the magnetic unit cell. These magnetic atoms are arranged along the $[0\bar{1}1]$, $[\bar{1}01]$, or $[1\bar{1}0]$ directions in the $\langle 111\rangle$ oriented stacking plane. At the same time, the easy axis of magnetic anisotropy in the AFM layer runs along the same direction in each unit cell, and the easy axis in the FM layer is $[1\bar{1}0]$. The configurations of atoms are equal in all of these three patterns, forming the ordered $L1_0$-type lattices. The single domain is composed of one of those three patterns, which includes 12×12 atoms in the stacking plane. The entire calculating model includes 3×3 domains, and the outer edge of the calculating region in the $\langle 111\rangle$ stacking plane is defined as the periodic boundary condition.

The frustrated spins are caused by the geometry of the magnetic atoms at the domain boundaries. As a result, in contrast to the loop in Fig. 3, the calculated magnetization loop is actually shifted by the unidirectional exchange-bias field even in the ordered $L1_0$-type alloy systems as shown in Fig. 9. Therefore, it is confirmed that the introduction of the frustrated spins causes the unidirectional exchange-bias field. The thickness dependence of the exchange-bias field is given in Fig. 10. The unidirectional exchange-bias field decreases

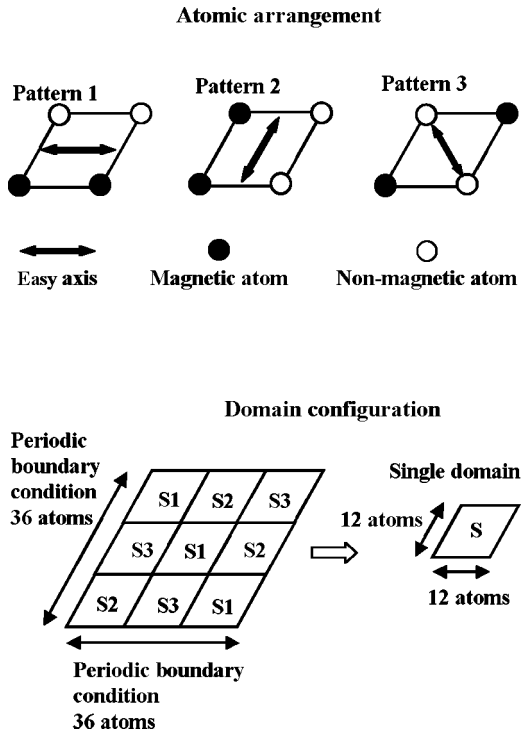

FIG. 8. Schematic drawing of the multidomains model.

with decreasing the AFM layer thickness, coming close to zero below a certain critical thickness. The maximum value of coercivity is obtained near such a critical thickness, accompanied by a sharp peak. These critical behaviors are very similar to the results of the unidirectional exchange-bias field H_u in Fig. 6.

The depth profile of the spin configuration is shown in Fig. 11, where the AFM layer thickness is 20 ML in Fig. 11(a) and 40 ML in Fig. 11(b). The magnetizations are measured along the direction of the applied field and they are averaged over the net plane in each depth. The stacked planes in depth from 1 to 9 ML correspond to the FM layer. The stacked planes in depth from 10 to 29 ML correspond to the AFM layer in Fig. 11(a), and the stacked planes in depth from 10 to 49 ML correspond to the AFM layer in Fig. 11(b).

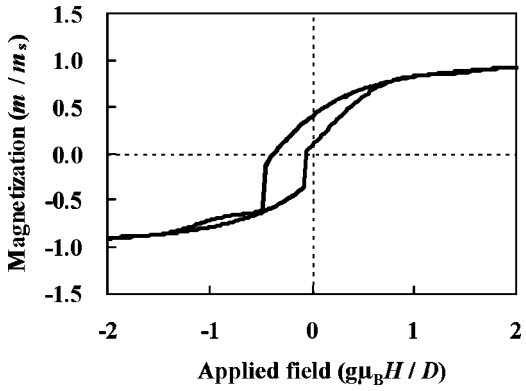

FIG. 9. The magnetization loop of the FM layer stacked on the ordered $L1_0$-type AFM layer in the multidomains model.

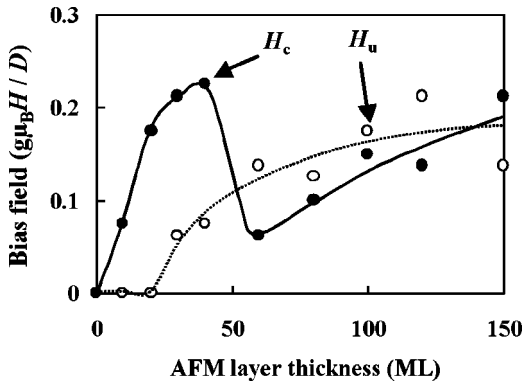

FIG. 10. The thickness dependence of the unidirectional exchange-bias field H_u (dashed line) and coercivity H_C (thick line) of the FM/AFM bilayer of the ordered $L1_0$-type alloy.

The thicknesses of 20 and 40 MLs of the AFM layer, respectively, represent the conditions below and above the critical thickness, where the magnetization loop shift appears. In the former case in Fig. 11(a), there is a small rotation of spins in the AFM layer. Switching the external field from $+H_{app}$ to $-H_{app}$, the magnetization at the site I changes from positive to negative and vice versa at the site II. As a result, the magnetic structure shows a symmetric configuration in the applied field. In the latter case in Fig. 11(b), on the other hand, the spins at the sites I and II remain in the same direction without switching, e.g., the magnetization at the site I always indicates a positive value in the AFM layer regardless under the positive $+H_{app}$ and negative $-H_{app}$ applied fields. Then, the domain wall structure is formed in the AFM layer, and the wall width changes from 10 to 30 ML in alternative applied fields. Therefore, this magnetic structure shows an asymmetric configuration in the applied field. Obviously, the symmetric change of the magnetic configuration in the applied field represents the absence of the unidirectional exchange-bias field H_u, and this asymmetric configuration in the applied field results in the magnetization loop shift. Also, this domain wall motion induces the difference between the magnetic energy in the bilayer under the positive and negative fields. The magnetic energies are plotted as a function of the applied field in Figs. 12(a) and 12(b) for 20 and 40 ML of the AFM layers, respectively. Symmetric and asymmetric curves of the magnetic energies are obtained for the thinner and the thicker AFM layers, respectively.

As discussed above, we have demonstrated that the introduction of the frustrated spins into the collinear spin configuration of the AFM layer can develop the unidirectional exchange-bias field. The formation of the magnetic domain wall parallel to the interface of the FM and AFM bilayers is also necessary. These prerequisites, the frustrated spins and the domain wall, are common to both the ordered $L1_0$-type and disordered γ-phase AFM systems. In addition, the multidomain structures to create the frustrated spins are also required for the collinear spin structure in the ordered $L1_0$-type AFM layer. The AFM domains correspond to the domains in Fig. 8, that is to say, the domain structures are in part similar to the random-field model by Malozemoff.[2] The random-field model stands within the framework of the Ising spin

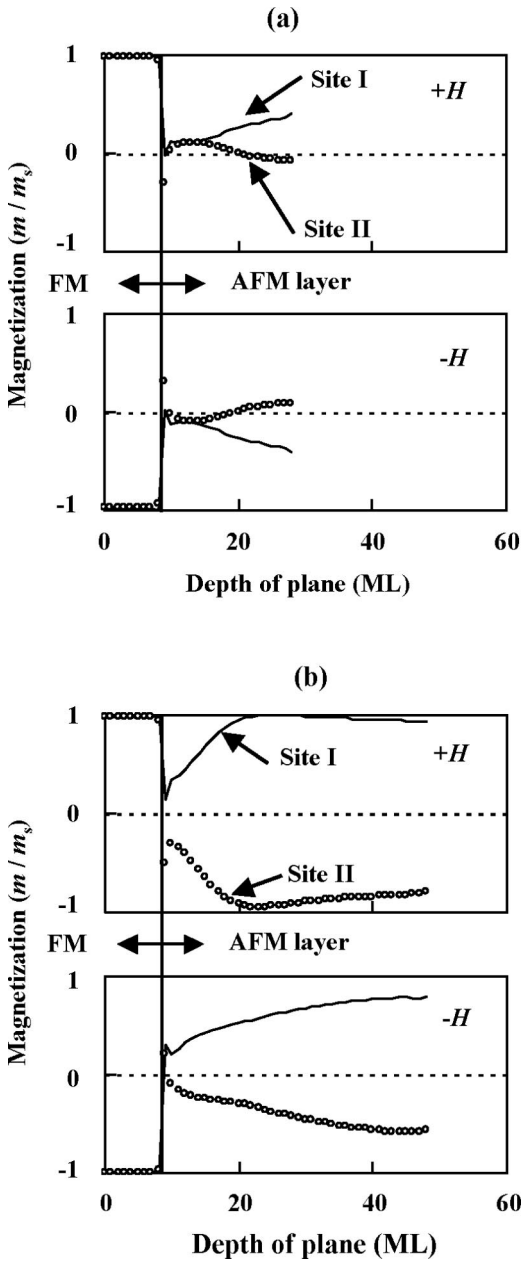

FIG. 11. The depth profile of magnetizations on stacked planes in the multidomain model in the FM/AFM bilayer of the $L1_0$-type ordered alloy. (a) Depth from 1 to 9 corresponds to the FM layer with 9 ML and the depth from 10 to 29 corresponds to the AFM layer with 20 ML, (b) Depth from 1 to 9 corresponds to the FM layer with 9 ML and the depth from 10 to 49 corresponds to the AFM layer with 40 ML. Note that the AFM layer thicknesses correspond to below and above the critical thickness for the exchange-bias field phenomenon.

system. In a wide sense, however, the AFM domain and the perpendicular domain wall in the random-field model can be regarded as the present multidomains model. The domains in Fig. 8 also correspond to grains in the polycrystalline models by Nishioka *et al.*[16] and Tsunoda and Takahashi.[17] Those two polycrystalline models include no influences of the frustrated spins at the interface. As a consequence, those polycrystalline models are naturally extended to the present model of

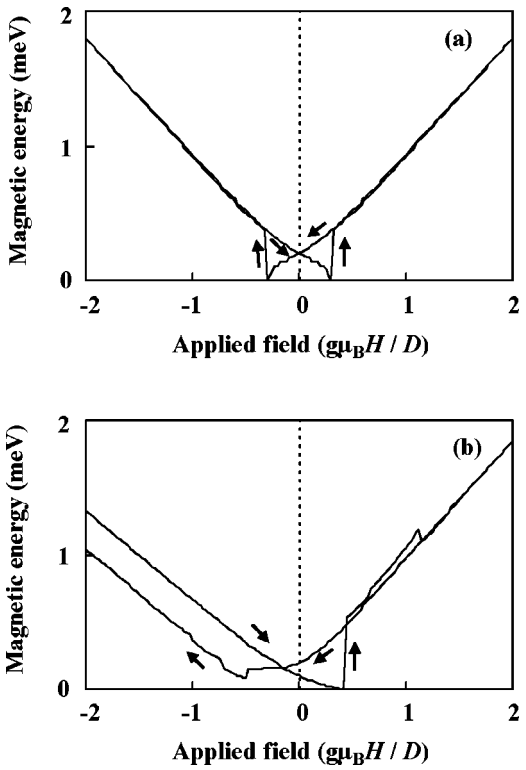

FIG. 12. The magnetic energy of the FM/AFM bilayer as a function of the applied field. (a) 20 ML thickness of the AFM layer, (b) 40 ML thickness of the AFM layer. Note that these thicknesses correspond to below and above the critical thickness for the exchange-bias field phenomenon.

the compensated interface by taking the influence of frustrated spins into consideration.

VI. SUMMARY

We have investigated the spin structure of FM and antiferromagnetic AFM bilayers and proposed the mechanism of the unidirectional exchange-bias field within the framework of the classical Heisenberg model. The noncollinear triple ($\equiv 3Q$) spin structure and the collinear AF-I spin structure are obtained in a disordered γ-phase AFM layer and an ordered $L1_0$-type AFM layer, respectively. The noncollinear $3Q$ spin structure in the AFM layer naturally induces the in-plane magnetization reversal (2D reversal), and the bilayer exhibits a magnetization loop shift. The 2D reversal process closely relates to the magnetic domain wall in the AFM layer parallel to the interface of the bilayer. The stability of such a domain wall formation in the applied field dominates the development of the unidirectional exchange-bias field. In this sense, the magnetic anisotropy energy in the AFM layer plays an important role, and the critical AFM thickness is dominated by such a domain wall width.

On the contrary, the unidirectional exchange-bias field is not developed by the simple collinear spin structure in the ordered $L1_0$-type AFM layer. In this case, the switching mode of the magnetization in the FM layer behaves as the 3D reversal process; perpendicular component of the spin

vector to the interface becomes finite during the magnetization reversal process, and the domain wall parallel to the interface is not created. For the noncollinear spin structure in the disordered γ-phase AFM layer, the prerequisites of the unidirectional exchange-bias field are the frustrated spins and the magnetic domain wall parallel to the interface. Therefore, we need to introduce the frustrated spins into the ordered $L1_0$-type AFM layer because the collinear spin structure has no frustrated spins. Accordingly, the present multidomains model is able to develop the unidirectional exchange-bias field originated from the frustrated spins at the AFM domain boundaries. Furthermore, the present model can also create the magnetic domain wall parallel to the interface, and the critical thickness for the formation of the unidirectional exchange-bias field is dominated by such a domain wall width in analogy with the noncollinear AFM system.

*Electronic address: chiharu_mitsumata@hitachi-metals.co.jp

[1] W.H. Meiklejohn and C.P. Been, Phys. Rev. **102**, 1413 (1956).
[2] A.P. Malozemoff, Phys. Rev. B **35**, 3679 (1987).
[3] N.C. Koon, Phys. Rev. Lett. **78**, 4865 (1997).
[4] T.C. Schulthess and W.H. Butler, Phys. Rev. Lett. **81**, 4516 (1998).
[5] T.C. Schulthess and W.H. Butler, J. Appl. Phys. **85**, 5510 (1999).
[6] J.-V. Kim and R.L. Stamps, Appl. Phys. Lett. **79**, 2785 (2001).
[7] U. Nowak, A. Misra, and K.D. Usadel, J. Appl. Phys. **89**, 7269 (2001).
[8] Y. Sakurai, H. Kitatani, T. Ishiguro, Y. Ichinose, and N.S. Kazama, IEEE Trans. Magn. **29**, 3879 (1993).
[9] D. Mauri, H.C. Siegmann, P.S. Bagus, and E. Kay, J. Appl. Phys. **62**, 3047 (1987).
[10] H. Xi, R.M. White, and S.M. Resende, Phys. Rev. B **60**, 14 837 (1999).
[11] H. Xi and R.M. White, IEEE Trans. Magn. **36**, 2635 (2000).
[12] J. Geshev, Phys. Rev. B **62**, 5627 (2000).
[13] H. Suhl and I.K. Schuller, Phys. Rev. B **58**, 258 (1998).
[14] T.C. Schulthess and W.H. Butler, J. Appl. Phys. **83**, 7225 (1998).
[15] K. Nakamura, A.J. Freeman, D.S. Wang, L. Zhong, and J. Fernandez-de-Castro, Phys. Rev. B **65**, 012402 (2001).
[16] K. Nishioka, C. Hou, H. Fujiwara, and R.D. Metzger, J. Appl. Phys. **80**, 4528 (1996).
[17] M. Tsunoda and M. Takahashi, J. Appl. Phys. **87**, 6415 (2000).
[18] J.S. Kasper and J.S. Kouvel, J. Phys. Chem. Solids **11**, 231 (1959).
[19] E. Krén, E. Nagy, I. Nagy, L. Pál, and P. Szabó, J. Phys. Chem. Solids **29**, 101 (1968).
[20] E. Krén, G. Kádár, L. Pál, J. Sólyom, P. Szabó, and T. Tarnóczi, Phys. Rev. **171**, 574 (1968).
[21] A. Sakuma, R.Y. Umetsu, and K. Fukamichi, Phys. Rev. B **66**, 014432 (2002).
[22] A. Sakuma, K. Fukamichi, K. Sasao, and R.Y. Umetsu, Phys. Rev. B **67**, 024420 (2003).
[23] R.F.C. Farrow, R.F. Marks, G. Gider, A.C. Marley, and S.S.P. Parkin, J. Appl. Phys. **81**, 4986 (1997).
[24] M. Saito, Y. Kakihara, T. Watanabe, and N. Hasegawa, J. Magn. Soc. Jpn. **21**, 505 (1997).
[25] T. Lin, D. Mauri, N. Staud, C. Hwang, J.K. Howard, and G. Gorman, Appl. Phys. Lett. **65**, 1183 (1994).
[26] B.Y. Wong, C. Mitsumata, S. Prakash, D.E. Laughlin, and T. Kobayashi, J. Appl. Phys. **79**, 7896 (1996).
[27] A. Velosa, P.P. Fretas, N.J. Oliveira, J. Fernandes, and M. Ferreira, IEEE Trans. Magn. **34**, 2343 (1998).
[28] M. Lederman, IEEE Trans. Magn. **35**, 794 (1997).
[29] M. Tsunoda, Y. Tsuchiya, M. Konoto, and M. Takahashi, J. Magn. Magn. Mater. **171**, 29 (1997).
[30] H.N. Fuke, K. Saito, Y. Kamiguchi, H. Kwasaki, and M. Sahashi, J. Appl. Phys. **81**, 4004 (1997).
[31] R.D. Hempstead, S. Krongelb, and D.A. Thompson, IEEE Trans. Magn. **14**, 521 (1978).
[32] R. Jungblut, R. Coehoorn, M.T. Johnson, J. aan de Stegge, and A. Reinders, J. Appl. Phys. **75**, 6659 (1994).
[33] A.E. Berkowitz and K. Takano, J. Magn. Magn. Mater. **200**, 552 (1999).
[34] A. Sakuma, J. Magn. Magn. Mater. **187**, 105 (1998).
[35] J. Villain, R. Bidaux, J.-P. Carton, and R. Conte, J. Phys. (Paris) **41**, 1263 (1980).
[36] C.L. Henley, J. Appl. Phys. **61**, 3962 (1987).
[37] M.W. Long, J. Phys.: Condens. Matter **1**, 2857 (1989).
[38] Y. Endo and Y. Ishikawa, J. Phys. Soc. Jpn. **30**, 1614 (1971).
[39] A. Sakuma, J. Phys. Soc. Jpn. **67**, 2815 (1998).
[40] A. Tanaka, Y. Shimizu, H. Kishi, K. Nagasaka, and M. Oshiki, IEEE Trans. Magn. **33**, 3592 (1997).